American Mineralogist, Volume 89, pages 1752–1762, 2004

Crystal chemistry and paragenesis of compositionally unique (Al-, Fe-, Nb-, and Zr-rich) titanite from Afrikanda, Russia

ANTON R. CHAKHMOURADIAN*

Department of Geological Sciences, University of Manitoba, Winnipeg, Manitoba R3T 2N2, Canada

ABSTRACT

Titanite is a common accessory mineral in silicocarbonatite from the Afrikanda alkaline-ultramafic complex, Kola Peninsula, Russia. In addition to large crystals (described elsewhere), this rock contains microscopic crystals and aggregates of titanite intimately associated with, or mantling, primary Ti minerals (perovskite, ilmenite, magnetite, and garnets). The microcrysts commonly exhibit complex zoning patterns that represent a combination of oscillatory, core-rim, and/or sectorial zoning. Eight varieties of microcrystic titanite, differing in chemical composition, mode of occurrence, and style of zoning, can be distinguished. Most of the compositions have >20% of the Ti site occupied by Al, Fe, Nb, Zr, or a combination thereof, whereas substitutions at the Ca site are limited to <2%. Analysis of element correlations and Raman spectra suggests that the compositional diversity of the titanite arises from the following substitutions: $(Al,Fe^{3+})(OH)Ti_{-1}O_{-1}$, $(Al,Fe^{3+})NbTi_{-2}$, $Al(OH)Zr_{-1}O_{-1}$, and $ZrTi_{-1}$. Using the end-member notation, different varieties of the microcrysts contain up to 20 mol% $CaFeSiO_4(OH)$, 37 mol% $CaAlSiO_4(OH)$, 35 mol% $Ca(Al_{0.5}Nb_{0.5})SiO_5$, and 26 mol% $CaZrSiO_5$. This compositional diversity is unparalleled by titanite from any other locality or rock type, including material from three other Kola carbonatites examined in the present work (Kovdor, Turiy Mys, and Seblyavr). All compositional varieties of the microcrystic titanite crystallized at late evolutionary stages as products of reaction between the primary Ti minerals and a deuteric aqueous fluid at temperatures near 200 °C, weakly acidic pH, and $a(H_4SiO_4^0) > 10^{-4}$. Under these conditions, the earlier-formed Zr minerals zirconolite and zircon were unstable and underwent extensive re-equilibration with the fluid, involving partial removal of Zr. Implications of these data for the safe disposal of nuclear waste are discussed. The structure of zirconian titanite was examined using a synthetic sample of analogous composition (25 mol% $CaZrSiO_5$). Its structure was refined by the Rietveld method from X-ray powder diffraction data in space group $A2/a$ [a 7.1119(7), b 8.7724(8), and c 6.6007(6) Å, β 113.569(4)°]. Reflections violating A centering and/or indicative of Ti-Zr ordering were not observed, and attempts to refine the structure in two alternative space groups ($P2_1/a$ and $P2_1$) were unsuccessful.

INTRODUCTION

Titanite is one of the most common and paragenetically supple titanium minerals in the lithosphere. It is found in rocks of different chemistry and provenance, from upper-mantle xenoliths (Schulze 1990) to diagenetic environments (Hole et al. 1992). It is a characteristic accessory and, in some cases, major constituent of alkaline silicate rocks and associated carbonatites, and is commonly used to constrain the crystallization conditions and age of these rocks (e.g., Peterson 1989; Villeneuve and Relf 1998; Chakhmouradian and Zaitsev 2002). Despite the ubiquitous nature and petrologic significance of titanite in alkaline and carbonatitic rocks, there are very few published studies of the compositional variation and crystal chemistry of this mineral. The available data suggest that titanite from these types of rocks may contain significant amounts of Sr, rare-earth elements (REE), and Zr (Russell et al. 1994; Chakhmouradian and Mitchell 1999; Chakhmouradian and Zaitsev 2002). Structural tolerance of titanite to these elements has important implications for immobilization of high-level nuclear waste in glass ceramics (see Discussion). Sr-, REE-, and Zr-doped $CaTiSiO_5$ has been synthesized at high temperatures (e.g., Stäuble and Bayer 1981a; Stefanovsky et al. 2000), but there is no information on the stability of these phases in low-temperature aqueous fluids, the type of conditions most relevant to the problem of nuclear-waste disposal.

During a systematic study of minerals hosting high-field-strength elements (HFSE) in carbonatites, several varieties of deuteric titanite with highly unusual compositional characteristics were identified in samples from a single occurrence of silicocarbonatite at Afrikanda in the Kola Peninsula, northwestern Russia. Some of these varieties (e.g., Fe- and Zr-rich) have unique compositions not previously reported for titanite from any type of rocks, whereas others (e.g., Nb- and Al-rich) have not been known to occur in carbonatites sensu lato. A detailed description of the occurrence and crystal chemistry of the Afrikanda titanite is provided below. Because the Zr-rich variety could not be examined using conventional X-ray diffraction methods due to the paucity of material, its compositional analogue was synthesized and structurally characterized in the present study. Possible implications of these data for nuclear-waste disposal are discussed.

* E-mail: chakhmou@ms.umanitoba.ca

Occurrence and paragenesis

The Afrikanda complex is a Devonian multiphase intrusion of ultramafic and alkaline rocks emplaced in Archean gneisses of the Fennoscandian Shield. The bulk of the intrusion consists of diverse modal and textural varieties of clinopyroxenite. Carbonatitic rocks are found predominantly in the central part of the complex, where they form veins and nests in the clinopyroxenites and olivinites. Silicocarbonatite is more common than calcite carbonatite, and comprises diopside, magnesiohastingsite, and calcite, with lesser amounts of perovskite, magnetite, titanite, richterite, chlorite, and ilmenite. This rock also contains a wide variety of accessory phases characteristic of carbonatites (sensu lato), including pyrochlore- and ancylite-group minerals, Na-bearing carbonates, and Zr-bearing oxides. Chakhmouradian and Zaitsev (2002, 2004) proposed that the carbonatitic rocks at Afrikanda are not related by either fractionation or liquid immiscibility to the clinopyroxenites and alkaline lithologies, and probably crystallized from an alkali-silica-rich carbonatitic melt derived from an independent mantle source.

Titanite is ubiquitous in the silicocarbonatite. Most common are honey-yellow wedge-like crystals up to several centimeters in length, associated with perovskite and confined to calcite pockets in the rock. Other "macro" varieties are lemon-yellow and dark brown crystals associated with zircon and chlorite, respectively. All three types also differ in chemical composition and unit-cell dimensions (Chakhmouradian and Zaitsev 2002). These varieties show minor to moderate deviation from the ideal formula ($CaTiSiO_4O$), principally owing to substitutions at the Ti site. The highest proportion of substituent elements (up to 15 at% Fe + Nb + Zr + Al) is found in the dark brown titanite.

A more detailed examination showed that, in addition to these "macro" varieties, the silicocarbonatite contains microscopic (typically <100 μm across) crystals and aggregates of titanite intimately associated with, or mantling, the primary Ti minerals (perovskite, ilmenite, magnetite, and titanian garnets). In all cases, the microcrystic titanite is embedded in, or developed at the contact with, calcite. Deuteric minerals associated with the microcrysts (both spatially and genetically) are loparite-(Ce), cerite-(Ce), ancylite-(Ce), hibschite, chlinochlore-chamosite, and Na-Ca zirconosilicates (see Appendix 1 for formulae). In general, the microcrysts show no evidence of resorption, chemical re-equilibration, or replacement by other minerals. In a single sample, a titanite mantle on ilmenite is partially replaced by rutile (confirmed by Raman microspectroscopy). The titanite microcrysts are wedge-shaped to elongate prismatic in habit and are typically intergrown as penetration twins, "sheaves," and radial aggregates. Lineage structures, shingle- and step-like sculpture on the crystal faces are very common (Fig. 1). In back-scattered electrons (BSE), this mineral shows significant variations in average atomic number (AZ) that, in most cases, represent an overlay of oscillatory, core-rim, and sectorial zoning (Figs. 2 and 3).

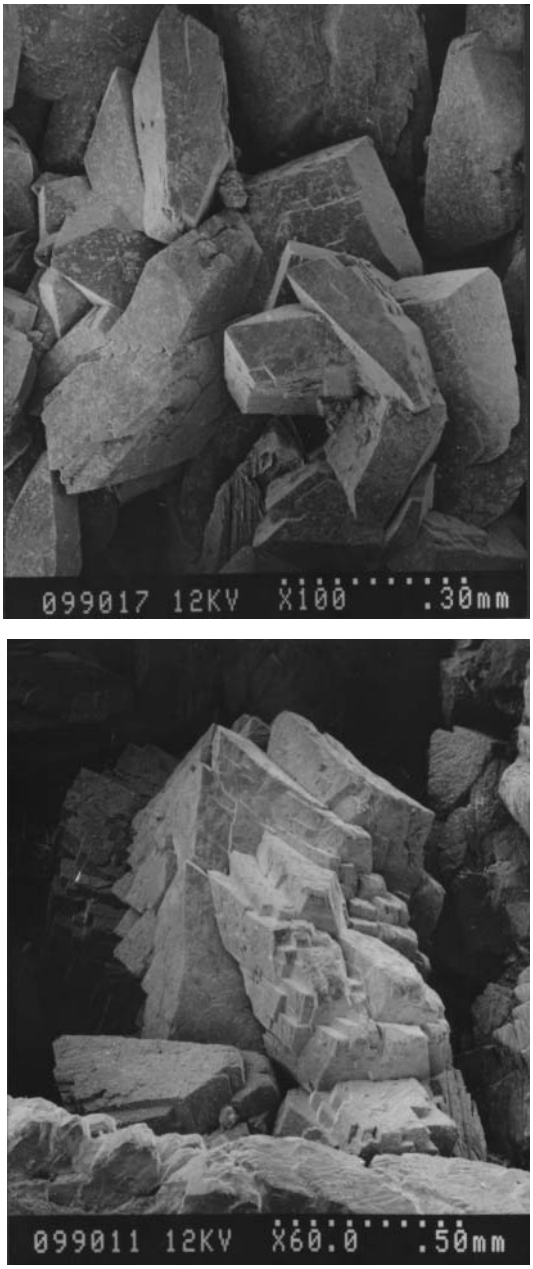

Figure 1. Crystal morphology of microcrystic titanite from Afrikanda. Note abundant lineage structures and twinning. Scanning-electron microscopy photograph.

Analytical methods

The mineral compositions were determined by wavelength-dispersive X-ray spectrometry using a CAMECA SX-50 electron-microprobe operated at 20 kV and 20 nA. The following standards were employed for the analysis: titanite (Si, Ca, Ti), albite (Na), fayalite (Fe), kyanite (Al), manganotantalite (Ta), spessartine (Mn), synthetic $ZrSiO_4$ (Zr), $HfSiO_4$ (Hf), $MnNb_2O_6$ (Nb), REE glasses (La, Ce, Nd), and $SrTiO_3$ (Sr). Raman spectra were collected from different zones in randomly oriented microcrysts using a Renishaw Raman microspectrometer equipped with a 785 nm diode laser and an automated *x*-*y* stage. The spectra were collected in confocal mode in intervals from 300–1200 and 2800–3500 cm^{-1}; crystalline Si was used as a calibration standard.

Crystal chemistry

Eight compositional varieties of microcrystic titanite were identified in approximately 20 samples of silicocarbonatite examined in the present study (see Table 1 for representative analy-

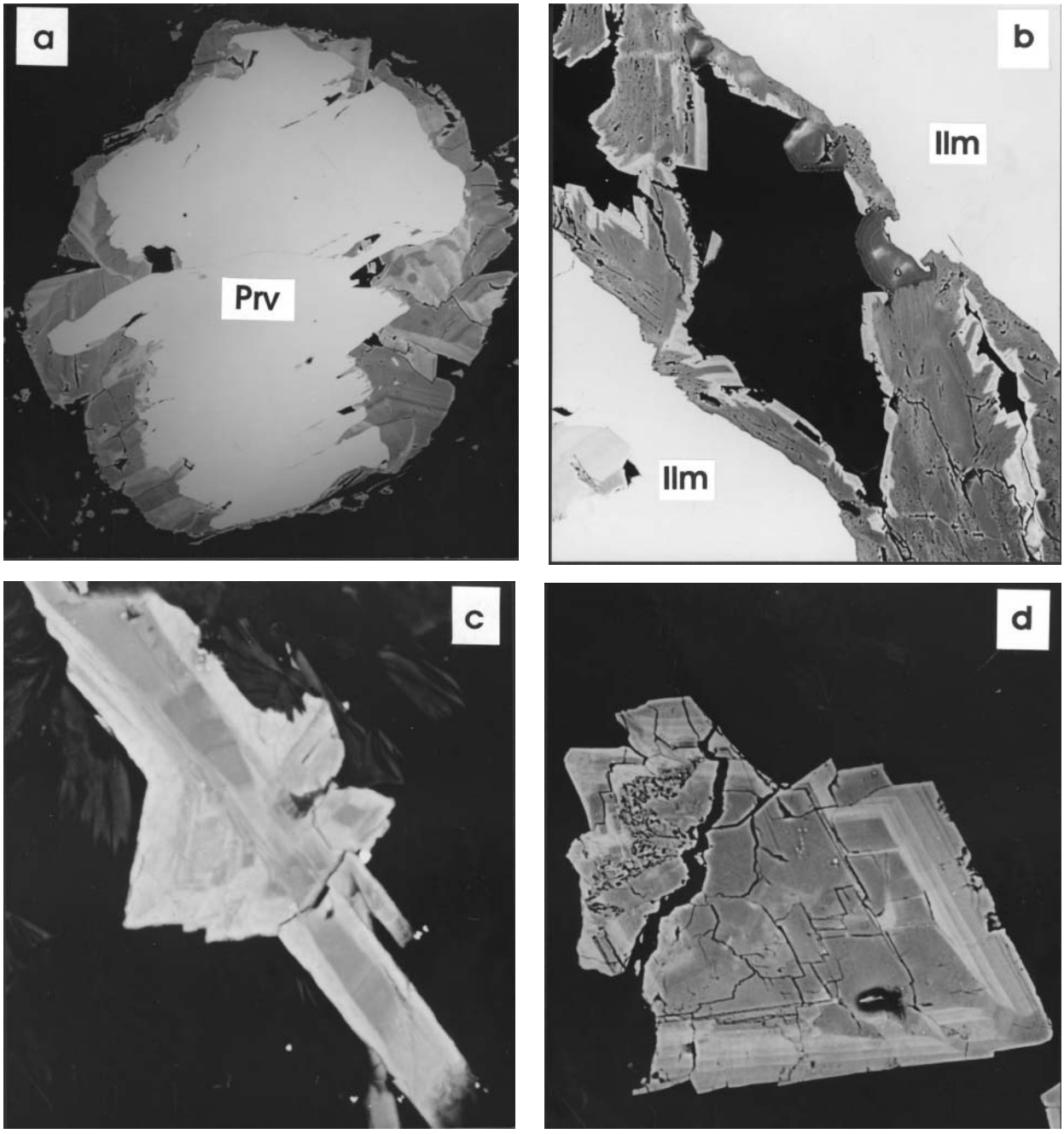

FIGURE 2. Microcrystic titanite from Afrikanda: Characteristic textures and zoning patterns. (**a**) Variety 1 mantling perovskite (white), width of the field of view (FOV) is 550 µm; (**b**) variety 3 mantling ilmenite (white), FOV 190 µm; (**c**) variety 5, FOV 80 µm; (**d**) variety 6, FOV 130 µm.

ses). (1) The most common variety comprises reaction mantles on, pseudomorphs after, and fracture fillings in perovskite (Fig. 2a). This titanite exhibits sectorial and fine oscillatory zoning, in which the low-AZ sectors are enriched in Al (5.3–8.5 wt% Al_2O_3) relative to the high-AZ sectors (<5.0 wt% Al_2O_3). (2) Fracture fillings in titaniferous magnetite and pseudomorphs after exsolution lamellae of ilmenite are invariably enriched in Fe (4.4–8.3 wt% Fe_2O_3). The published Mössbauer data indicate that, within the accuracy of the method, non-metamict titanite contains only Fe^{3+} substituting in the Ti site; detectable Fe^{2+} has been reported in Precambrian samples showing significant radiation damage (Muir et al. 1984; Hawthorne et al. 1991). Hence, we assume that all Fe in the Afrikanda material is trivalent. (3) Mantles on platy ilmenite, and clusters of wedge-shaped microcrysts around this ilmenite (Fig. 2b) are strongly zoned with Al enrichment in the core (8.1–10.0 wt% Al_2O_3), and Nb enrichment coupled with relative Al depletion in the high-AZ rim (7.6–11.4 wt% Nb_2O_5, 3.2–6.4 wt% Al_2O_3). Subtle oscillatory zoning is

present in both core and rim. In some of the crystals, the Nb_2O_5 and Al_2O_3 contents decrease to less than 3.0 wt% in the low-AZ outermost rim. (4) Microcrysts alternate between Zr-rich (7.8–9.8 wt% ZrO_2) and Nb-Al-rich zones (5.6–6.1 wt% Nb_2O_5; 3.8–4.8 wt% Al_2O_3) in the core, and low to moderate concentrations of these elements in the low-AZ rim. (5) Elongate microcrysts contain high levels of Al in the low-AZ core (5.2–10.2 wt% Al_2O_3), and contain high levels of Zr and Hf in the high-AZ rim (11.4–15.3 wt% ZrO_2, up to 0.5 wt% HfO_2). This core-to-rim pattern is accompanied by more subtle sectorial and oscillatory

TABLE 1. Representative compositions of microcrystic titanite from Afrikanda

Wt%	1	2	3	4	5	6	7	8	9	10
Na_2O	0.08	0.09	0.09	0.16	n.d	n.d	n.d	0.11	n.d	0.14
CaO	29.08	29.33	28.04	28.04	29.16	28.61	28.24	27.85	27.57	28.09
La_2O_3	n.d	n.d	0.04	n.d	n.d	n.d	n.d	n.d	n.d	n.d
Ce_2O_3	n.d	0.08	0.67	0.46	n.d	0.48	0.51	n.d	n.d	n.d
Nd_2O_3	n.d	n.d	0.03	0.45	n.d	n.d	n.d	n.d	n.d	n.d
MnO	0.06	n.d	n.d	n.d	n.d	n.d	n.d	n.d	n.d	n.d
TiO_2	34.02	31.20	35.92	31.39	27.99	29.12	34.65	31.25	32.28	33.66
Nb_2O_5	0.34	0.39	0.50	3.08	1.59	1.54	0.24	n.d	0.07	n.d
Fe_2O_3*	0.62	1.04	1.07	0.99	0.20	0.32	1.72	8.29	7.47	4.44
Al_2O_3	5.29	6.85	3.54	4.99	8.46	7.25	3.32	0.86	0.44	1.79
SiO_2	30.80	31.05	30.17	30.49	31.44	30.95	30.23	30.07	30.17	30.33
Total	100.29	100.03	100.07	100.05	98.84	98.27	98.91	98.43	98.00	98.45
Structural formulae calculated on the basis of 3 cations										
Na	0.005	0.006	0.006	0.010	–	–	–	0.007	–	0.009
Ca	0.988	0.990	0.970	0.971	0.991	0.987	0.986	0.985	0.983	0.987
La	–	–	–	–	–	–	–	–	–	–
Ce	–	0.001	0.008	0.005	–	0.006	0.006	–	–	–
Nd	–	–	–	0.005	–	–	–	–	–	–
Σ	0.993	0.997	0.984	0.992	0.991	0.993	0.992	0.992	0.983	0.996
Mn	0.002	–	–	–	–	–	–	-	–	–
Ti	0.810	0.739	0.873	0.763	0.668	0.705	0.849	0.776	0.808	0.830
Nb	0.005	0.006	0.007	0.045	0.023	0.022	0.004	–	0.001	–
Fe*	0.015	0.025	0.026	0.024	0.005	0.008	0.042	0.206	0.187	0.110
Al_{VI}	0.175	0.233	0.110	0.176	0.313	0.272	0.113	0.026	0.017	0.064
Σ	1.007	1.003	1.016	1.008	1.009	1.007	1.008	1.008	1.013	1.004
Al_{IV}	0.023	0.021	0.025	0.014	0.003	0.003	0.015	0.007	–	0.005
Si	0.977	0.979	0.975	0.986	0.997	0.997	0.985	0.993	1.004	0.995
Σ	1.000	1.000	1.000	1.000	1.000	1.000	1.000	1.000	1.004	1.000

Note: Compositions: 1–4 zoned Al-rich titanite 1 replacing perovskite (Fig. 2a): 1–2 low-AZ zones, 3–4 high-AZ zones; 5–7 Al-rich titanite filling fracture in perovskite; 8–10 Fe-rich titanite 2 replacing ilmenite lamellae in magnetite.
* Total Fe expressed as Fe_2O_3; n.d = not detected.

TABLE 1.—*Continued*

Wt%	11	12	13	14	15	16	17	18	19	20
Na_2O	0.04	n.d	n.d	0.23	0.13	0.08	n.d	0.12	0.14	0.29
CaO	29.77	29.37	29.53	27.65	27.82	27.44	28.82	27.77	28.27	28.27
La_2O_3	n.d	n.d	n.d	n.d	n.d	0.22	n.d	n.d	n.d	n.d
Ce_2O_3	n.d	n.d	n.d	n.d	n.d	0.30	n.d	n.d	n.d	n.d
MgO	n.d	n.d	n.d	n.d	n.d	n.d	n.d	n.d	n.d	0.14
TiO_2	26.75	27.52	29.16	28.32	23.98	22.61	32.41	30.97	27.07	31.47
ZrO_2	n.d	0.24	n.d	1.23	0.58	0.88	0.13	8.89	2.88	0.41
Nb_2O_5	0.09	0.19	0.36	7.63	9.97	11.37	2.74	0.37	5.73	3.52
Fe_2O_3*	0.15	0.28	0.54	2.33	1.02	1.00	2.86	0.51	0.81	2.25
Al_2O_3	9.96	9.23	8.14	3.24	6.39	6.13	2.55	1.18	4.46	2.76
SiO_2	31.04	30.61	31.24	29.09	28.57	28.43	29.83	29.99	30.32	30.87
Total	97.80	97.44	98.97	99.72	98.46	98.46	99.34	99.80	99.68	99.98
Structural formulae calculated on the basis of 3 cations										
Na	0.002	–	–	0.015	0.008	0.005	–	0.008	0.009	0.018
Ca	1.007	1.004	0.999	0.987	0.996	0.994	1.012	0.997	0.997	0.984
La	–	–	–	–	–	0.003	–	–	–	–
Ce	–	–	–	–	–	0.004	–	–	–	–
Σ	1.009	1.004	0.999	1.002	1.004	1.006	1.012	1.005	1.006	1.002
Mg	–	–	–	–	–	–	–	–	–	0.007
Ti	0.635	0.659	0.693	0.709	0.603	0.575	0.799	0.780	0.671	0.769
Zr	–	0.004	–	0.020	0.009	0.015	0.002	0.145	0.046	0.006
Nb	0.001	0.003	0.005	0.115	0.151	0.174	0.041	0.006	0.086	0.052
Fe*	0.004	0.007	0.013	0.058	0.026	0.025	0.070	0.013	0.020	0.055
Al_{VI}	0.351	0.323	0.290	0.096	0.207	0.205	0.076	0.047	0.171	0.106
Σ	0.991	0.996	1.001	0.998	0.996	0.994	0.988	0.991	0.994	0.995
Al_{IV}	0.020	0.024	0.013	0.031	0.045	0.039	0.022	–	0.002	–
Si	0.980	0.976	0.987	0.969	0.955	0.961	0.978	1.004	0.998	1.003
Σ	1.000	1.000	1.000	1.000	1.000	1.000	1.000	1.004	1.000	1.003

Notes: Compositions: 11–17 zoned Al- and Nb-rich titanite 3 replacing discrete ilmenite (Fig. 2b): 11–13 low-AZ Al-rich core, 14-16 high-AZ Nb-rich rim, 17 outermost low-AZ zone relatively poor in Al and Nb; 18–19 core and 20 rim of Al-Nb-Zr-rich titanite 4.
* Total Fe expressed as Fe_2O_3; n.d = not detected.

TABLE 1.—Continued

Wt%	21	22	23	24	25	26	27	28	29	30	31
Na_2O	n.d	0.02	n.d	0.14	0.33	0.37	0.36	n.d	n.d	0.33	0.02
CaO	29.76	28.44	28.47	27.43	26.39	26.64	26.26	27.16	29.15	27.15	28.88
Ce_2O_3	n.d	n.d	n.d	n.d	n.d	n.d	n.d	n.d	n.d	0.95	0.29
Nd_2O_3	n.d	n.d	n.d	n.d	n.d	n.d	n.d	n.d	n.d	1.58	n.d
TiO_2	25.74	31.49	29.20	29.00	28.85	28.44	27.67	26.71	34.49	33.68	34.96
ZrO_2	0.28	1.16	3.98	8.65	11.39	13.18	14.90	15.31	0.17	0.28	n.d
HfO_2	n.d	n.d	0.23	0.33	0.38	0.42	0.45	0.46	n.d	n.d	n.d
Nb_2O_5	0.05	n.d	0.14	0.20	0.33	0.36	0.28	0.07	0.04	1.97	0.36
Fe_2O_3*	0.05	0.41	0.28	0.26	0.31	0.17	0.30	0.13	3.19	3.34	4.94
Al_2O_3	10.21	5.46	5.23	3.14	1.51	0.68	0.69	1.21	2.54	1.18	0.61
SiO_2	31.03	30.56	30.86	29.17	28.66	28.84	28.74	28.89	30.21	29.87	30.19
Total	97.12	97.54	98.59	98.32	98.15	99.10	99.65	99.94	99.79	100.33	100.25
Structural formulae calculated on the basis of 3 cations											
Na	–	0.001	–	0.009	0.022	0.025	0.024	–	–	0.021	0.001
Ca	1.012	0.993	0.996	0.991	0.974	0.983	0.971	1.001	1.009	0.961	1.007
Ce	–	–	–	–	–	–	–	–	–	0.011	0.004
Nd	–	–	–	–	–	–	–	–	–	0.019	–
Σ	1.012	0.994	0.996	1.000	0.996	1.008	0.995	1.001	1.009	1.012	1.012
Ti	0.615	0.772	0.722	0.736	0.747	0.736	0.718	0.691	0.838	0.837	0.856
Zr	0.004	0.018	0.063	0.142	0.192	0.221	0.251	0.257	0.003	0.005	–
Hf	–	–	0.002	0.003	0.004	0.004	0.004	0.004	–	–	–
Nb	0.001	–	0.002	0.003	0.005	0.006	0.004	0.001	–	0.030	0.005
Fe*	0.001	0.010	0.007	0.007	0.008	0.004	0.008	0.003	0.077	0.083	0.121
Al_{VI}	0.367	0.206	0.201	0.109	0.048	0.021	0.020	0.043	0.073	0.033	0.006
Σ	0.988	1.006	0.997	1.000	1.004	0.992	1.005	0.999	0.991	0.988	0.988
Al_{IV}	0.015	0.004	–	0.016	0.013	0.007	0.008	0.006	0.024	0.013	0.017
Si	0.985	0.996	1.007	0.984	0.987	0.993	0.992	0.994	0.976	0.987	0.983
Σ	1.000	1.000	1.007	1.000	1.000	1.000	1.000	1.000	1.000	1.000	1.000

Note: Compositions: 21–28 zoned Al- and Zr-rich titanite 5 (Fig. 2c): 21–22 low-AZ Al-rich core, 23–24 intermediate zones, 25–28 high-AZ Zr-rich rim; 29–31 low-AZ core, high-AZ intermediate zone and rim of titanite 6 encrusting titaniferous magnetite (Fig. 2d).
* Total Fe expressed as Fe_2O_3; n.d = not detected.

zoning (Fig. 2c). (6) Wedge-shaped microcrysts fringe margins of magnetite crystals, and they combine core-rim, oscillatory, and sectorial zoning (Fig. 2d). Their low-AZ core is enriched in Al, the high-AZ intermediate zone in Nb and REE, and the rim in Fe with respect to one another. (7) Spherulitic titanite associated with magnetite and perovskite shows a combination of sectorial and oscillatory zoning, and evidence of multiple growth episodes (Fig. 3). The relatively low-AZ areas comprise alternating Al- and Fe-rich zones (up to 4.8 and 7.3 wt% respective oxides), whereas the high-AZ areas are enriched in Nb (5.8–7.8 wt% Nb_2O_5). (8) Thin (<20 μm) mantles on shorlomite and titanian andradite contain 0.6–2.6 wt% ZrO_2, and are relatively poor in Al, Fe, and Nb. The Zr content is highest near inclusions of baddeleyite and zirconolite enclosed in the titanite (see Appendix 1 for formulae).

Each of these varieties appears to be restricted to a certain paragenetic microenvironment localized in small volumes (<1 cm^3) throughout the rock. It is not uncommon to find two and even three varieties with contrasting compositions within a single electron-microprobe mount (~5 cm^2). The two ubiquitous minerals found in variable amounts in all of the parageneses are chlorite and hibschite. Titanite 1 is also accompanied by REE minerals (loparite, cerite, and ancylite), whereas varieties (4), (5), and (8) are accompanied by zirconosilicates (primarily gittinsite).

Most of the titanite compositions have >0.2 apfu Ti (atoms of Ti per formula unit) replaced by Al, Fe, Nb, Zr, or a combination thereof. The highest proportion of substituent elements (ca. 0.4 apfu) is observed in varieties 3 and 5 (Table 2). With one exception (Table 1, analysis 30), the microcrystic titanite exhibits very limited substitution at the Ca site (≤0.02 apfu). None of the varieties contain detectable F, but the presence of

TABLE 1.—Continued

Wt%	32	33	34	35	36	37	38
Na_2O	n.d	n.d	0.02	0.15	0.22	n.d	0.15
CaO	29.52	28.90	28.96	27.81	27.28	28.47	28.10
Ce_2O_3	n.d	n.d	0.14	0.25	0.81	n.d	n.d
TiO_2	31.68	30.43	36.75	30.20	30.11	29.21	36.36
ZrO_2	n.d	n.d	n.d	0.41	0.27	n.d	2.61
Nb_2O_5	0.50	0.66	0.60	7.77	6.82	5.71	n.d
Fe_2O_3*	2.18	6.84	2.55	3.30	3.17	2.77	1.78
Al_2O_3	4.71	1.99	1.12	1.20	1.20	3.03	0.44
SiO_2	31.52	31.07	31.26	30.46	30.01	30.60	30.48
Total	100.11	99.89	101.40	101.55	99.90	99.79	99.92
Structural formulae calculated on the basis of 3 cations							
Na	–	–	0.001	0.010	0.014	–	0.009
Ca	1.005	1.002	0.995	0.983	0.978	1.002	0.989
Ce	–	–	0.002	0.003	0.010	–	–
Σ	1.005	1.002	0.998	0.996	1.002	1.002	0.998
Ti	0.757	0.740	0.886	0.749	0.758	0.722	0.898
Zr	–	–	–	0.006	0.005	–	0.042
Nb	0.007	0.010	0.009	0.116	0.103	0.085	–
Fe*	0.052	0.167	0.062	0.082	0.080	0.069	0.044
Al_{VI}	0.177	0.076	0.042	0.047	0.047	0.117	0.017
Σ	0.993	0.993	0.999	1.000	0.993	0.993	1.001
Si	1.002	1.005	1.003	1.004	1.005	1.005	1.001
Σ	1.002	1.005	1.003	1.004	1.005	1.005	1.001

Note: Compositions: 32–37 spherulitic titanite 7 (Fig. 3): 32–33 Al- and Fe-rich zones in oscillatory low-AZ areas, 34 low-AZ unzoned sector, 35–36 Nb-rich high-AZ sectors, 37 Nb-rich high-AZ rim; 38 titanite 8 rimming schorlomite.
* Total Fe expressed as Fe_2O_3; n.d = not detected.

$(OH)^{1-}$ groups is evident from well-resolved hydroxyl-stretching modes between 2900 and 3500 cm^{-1} in their Raman spectra. Although the amount of $(OH)^{1-}$ could not be determined for the lack of a suitable standard, the intensity of the peaks is highest in the most Fe- and Al-rich samples. Linear correlations are observed between Ti and (Al + Fe) in all samples, except for the Zr-rich zones of titanite 4 and 5, as well as between Nb and (Al + Fe) in the Nb-rich zones of varieties 3 and 4, between Zr

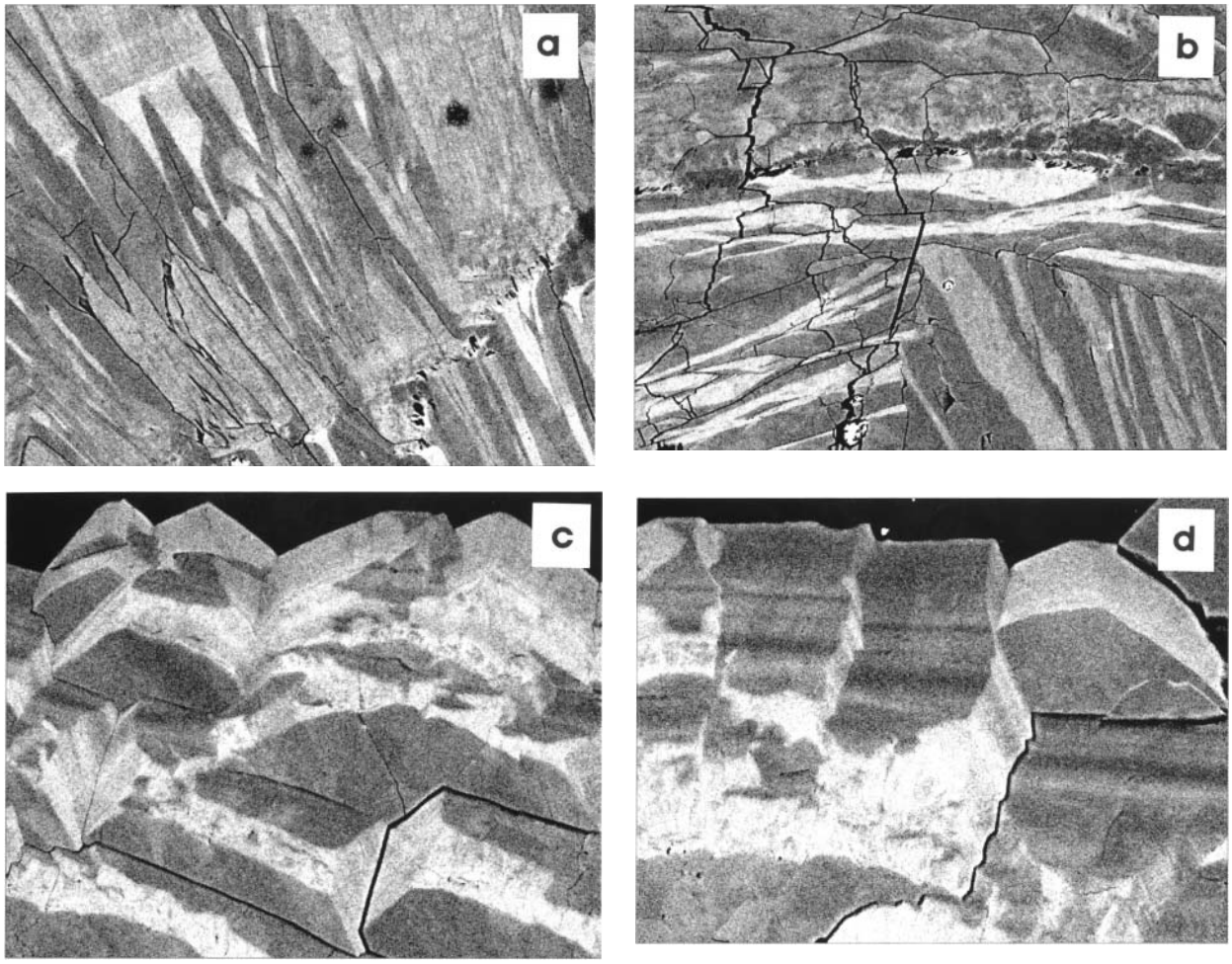

FIGURE 3. Complex combination of oscillatory, sectorial, and core-rim zoning in microcrystic titanite (variety 7). (**a**) Transition from predominantly sectorial zoning in the inner part of a spherulite to oscillatory zoning in the intermediate part, FOV 315 µm; (**b**) boundary between several spherulites showing the sectorial pattern as in (**a**) cross-cut in different orientations, FOV 380 µm; (**c**) and (**d**) outermost part of the spherulite showing a combination of oscillatory, sectorial, and core-rim zoning, FOV 200 and 160 µm, respectively.

TABLE 2. Structural parameters, selected interatomic distances, angles, and agreement factors for synthetic zirconian titanite, $Ca(Ti_{0.75}Zr_{0.25})SiO_5$

Atom	Wyckoff position	*x*	*y*	*z*	*B* (Å²)
Ca	4*e*	1/4	0.1662(7)	0	1.4(2)
Ti,Zr	4*a*	1/2	0	1/2	0.7(1)
Si	4*e*	3/4	0.182(1)	0	1.6(3)
O1	4*e*	3/4	0.070(1)	1/2	0.6(4)
O2	8*f*	0.921(1)	0.065(1)	0.177(1)	0.4(3)
O3	8*f*	0.385(1)	0.210(1)	0.397(1)	0.1(2)

Interatomic distances and angles:

Ca-O1	2.316 Å	O1-(Ti,Zr)-O2	87.6°
Ca-O2 (×2)	2.415 Å	O1-(Ti,Zr)-O2	92.4°
Ca-O3 (×2)	2.436 Å	O1-(Ti,Zr)-O3	87.6°
Ca-O2′ (×2)	2.639 Å	O1-(Ti,Zr)-O3	92.4°
(Ti,Zr)-O1 (×2)	1.880 Å (×2)	O2-(Ti,Zr)-O3	90.0°
(Ti,Zr)-O2 (×2)	2.055 Å	O2-Si-O2	104.0°
(Ti,Zr)-O3 (×2)	2.019 Å	O2-Si-O3	104.9°
Si-O2 (×2)	1.659 Å	O2-Si-O3	116.2°
Si-O3 (×2)	1.676 Å	O3-Si-O3	110.9°

Notes: Unit-cell parameters: *a* 7.1119(7) Å, *b* 8.7724(8), and *c* 6.6007(6) Å; β113.569(4)°; Agreement factors: R_{exp} 11.4%; R_p 9.8%; R_{wp} 12.7%; R_F 6.3%; χ^2 1.23; *DW* 1.67

and (Al + Fe) in titanite 4 and 5, and between Zr and Ti in the Al-poor areas of varieties 4, 5, and 7 (Fig. 4).

The above observations indicate that the compositional diversity of the microcrystic titanite results predominantly from the following substitutions: $(Al,Fe^{3+})(OH)Ti_{-1}O_{-1}$, $(Al,Fe^{3+})NbTi_{-2}$, $Al(OH)Zr_{-1}O_{-1}$, and $ZrTi_{-1}$. With the exception of the most Fe-, Al-, and Zr-rich varieties, two or more of these substitution mechanisms operate simultaneously, which explains the significant scatter of data points in Figure 4. Taking into account the data of Chakhmouradian and Zaitsev (2002), the compositional variation of both macro- and microcrysts can be expressed in terms of six hypothetical end-members with different cation populations at the Ti site: $CaTiSiO_5$, $CaAlSiO_4(OH)$, $CaFeSiO_4(OH)$, $CaZrSiO_5$, $Ca(Al_{0.5}Nb_{0.5})SiO_5$, and $Ca(Fe_{0.5}Nb_{0.5})SiO_5$. Contributions from $NaNbSiO_5$, $(Na_{0.5}REE_{0.5})TiSiO_5$, $REEAlSiO_5$, and other potential end-members involving substitutions at the Ca site are negligible and can be ignored for simplicity. The highest proportions of the "impurity" end-members observed among the Afrikanda

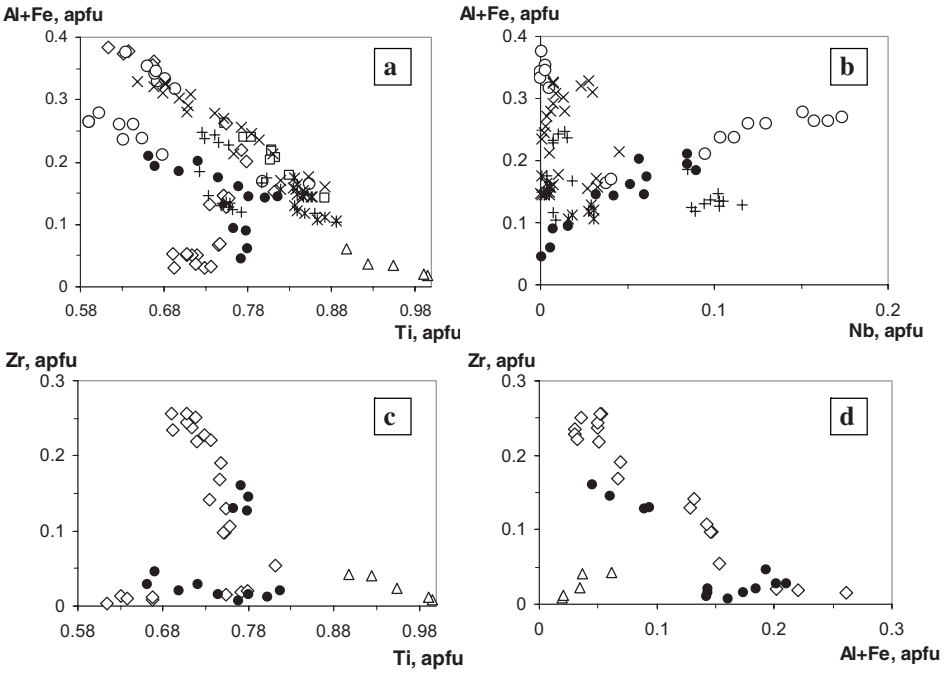

FIGURE 4. Compositional variation (apfu) of microcrystic titanite from Afrikanda. Individual varieties are denoted: X (1), squares (2), empty circles (3), solid circles (4), diamonds (5), snowflakes (6), crosses (7), and triangles (8).

samples are 20 mol% $CaFeSiO_4(OH)$ in titanite (2), 35 mol% $Ca(Al_{0.5}Nb_{0.5})SiO_5$ in titanite (3), and 37 mol% $CaAlSiO_4(OH)$ and 26 mol% $CaZrSiO_5$ in variety (5) (Fig. 5).

Unfortunately, the most compositionally unusual varieties of titanite (i.e., those containing >0.15 apfu Al, Fe, Nb, or Zr) occur in quantities insufficient for their examination by X-ray diffraction methods. However, their identity was confirmed by Raman microspectroscopy, as all obtained spectra contained a recognizable sequence of Si-O and Ti-O modes between 400 and 1000 cm^{-1} (cf. Heyns et al. 2000).

Synthetic zirconian titanite

Zirconian titanite was chosen for structural investigation because of its potential significance as a nuclear-waste form (see Discussion), and also because there is a general paucity of structural data for minerals showing extensive substitution of Ti by Zr. In Ti oxides and titanosilicates, the proportion of Zr rarely exceeds a few atomic per cent owing to the large (19%) difference between the ionic radii of $^{[VI]}Ti^{4+}$ and $^{[VI]}Zr^{4+}$ (Shannon 1976). A series of $Ca(Ti_{1-x}Zr_x)SiO_5$ compositions was previously synthesized by Stäuble and Bayer (1981a, 1981b), who determined that up to 53% of the Ti can be replaced by Zr. The structure of these compounds was not examined, but Stäuble and Bayer (1981a) remarked that the lattice symmetry changes from *A*-centered to primitive with increasing Zr content.

In the present study, a sample compositionally analogous to the most Zr-rich Afrikanda titanite ($CaTi_{0.75}Zr_{0.25}SiO_5$) was synthesized by melting a stoichiometric mixture of oven-dried $CaCO_3$, TiO_2, ZrO_2, and $SiO_2 \cdot nH_2O$ at 1500 °C, and cooling the melt slowly to room temperature. This synthesis method was preferred to the sintering employed by Stäuble and Bayer (1981a), because the latter yields many by-products. Crystallization of the melt produced a homogeneous sample, but the size of the titanite crystals was insufficient for their examination by single-crystal methods. Consequently, X-ray diffraction (XRD) powder data were collected using a Phillips 3710 diffractometer (Cu$K\alpha$ radiation, 2θ range 10–130°, $\Delta 2\theta = 0.02°$, time per step 2 s), and the structure of $CaTi_{0.75}Zr_{0.25}SiO_5$ was refined by the Rietveld method using the FULLPROF software (Rodriguez-Carvajal 1990).

Careful examination of the XRD pattern showed no reflections that would violate the *A*-centering ($k + l$ = odd); neither were present reflections indicating the loss of the *a* glide ($h0l$, where h = odd) and arising from cation ordering at the Ti site (Hollabaugh and Foit 1984). Consequently, the structure of zirconian titanite was refined in space group $A2/a$, using the atomic coordinates for high-temperature $CaTiSiO_5$ (Kunz et al. 2000) as a starting model, and assuming disordered distribution of 75% Ti and 25% Zr over the octahedrally coordinated positions. In the final cycles of refinement, a total of 35 instrumental, structural, and background parameters were refined simultaneously. The results of this refinement are listed in Table 2, along with selected interatomic distances and angles. Given that reflections violating the $A2/a$ symmetry could be undetectable on XRD powder patterns, attempts were made to refine the structure of $CaTi_{0.75}Zr_{0.25}SiO_5$ in the two alternative space groups, $P2_1/a$ and $P2_1$, using the parameters of Hollabaugh and Foit (1984) as starting models. Neither of these refinements yielded satisfactory results.

The crystal structure of titanite and isostructural minerals has been well characterized in the previously published literature (e.g., Ghose et al. 1991; Groat et al. 1996; Troitzsch et al. 1999), and will not be discussed here in detail. As can be expected, the unit cell of the zirconian titanite is significantly larger, whereas the β angle is smaller than for synthetic $CaTiSiO_5$ (e.g., Kunz et al. 2000). A similar decrease in β with increasing mean radius of the octahedrally coordinated cation is observed for other titanite

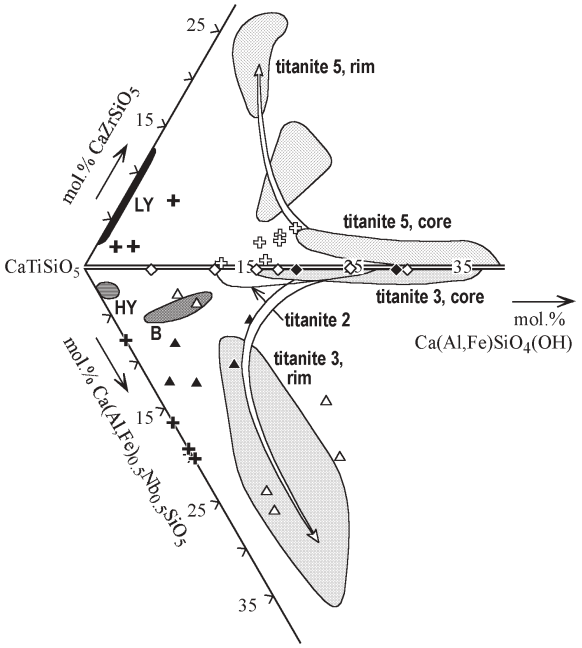

FIGURE 5. Compositional variation (mol%) of titanite from the Afrikanda silicocarbonatites: comparison with other localities and rock types. Fields HY, LY, and B are honey-yellow, lemon-yellow, and brown "macro" varieties of titanite from Afrikanda (Chakhmouradian and Zaitsev 2002). For clarity, only the compositions of microcrystic varieties 2, 3, and 5 are shown; data points for the other varieties plot within and between these fields. Diamonds stand for Al-rich titanite from metamorphic rocks of Montagne Noire (solid) and Salton Sea (empty), triangles for Nb-rich titanite from granitic pegmatites of Prašivá (solid) and Żólkiewka (empty), and crosses for titanite from syenitic rocks of Ilomba and Oldoinyo Lengai (solid), Tre Croci and Roccamonfina (empty). The diagram was constructed using the data of Gibert et al. (1990), Woolley et al. (1992), Enami et al. (1993), Dawson et al. (1995), Janeczek (1996), Uher et al. (1998), and Della Ventura et al. (1999).

compositions (e.g., Troitzsch et al. 1999). The refined unit-cell parameters (Table 2) are in good agreement with the data plotted on Figure 2 of Stäuble and Bayer (1981b). The mean (Ti,Zr)-O distance agrees well with that estimated from the ionic radii of Shannon (1976): 1.985 and 1.99 Å, respectively.

DISCUSSION AND COMPARISONS

Crystallization conditions

All compositional varieties of microcrystic titanite in the Afrikanda silicocarbonatite crystallized at late evolutionary stages as products of reaction between the primary Ti minerals (oxides and garnets) and a deuteric aqueous fluid. This process also affected the rock-forming mafic silicates (particularly magnesiohastingsite), leading to release of a substantial amount of Ca, Mg, Fe, Ti, and Al into the fluid. As many primary minerals in the host silicocarbonatite contained elevated levels of REE (perovskite and apatite), Nb (perovskite and ilmenite), Sr (calcite and apatite), Th (perovskite and zircon), Zr, and Hf (Zr oxides and zircon), these incompatible elements were also scavenged by the fluid. The rock-fluid interaction was not a simple one-step process, but instead involved a series of mineral replacement reactions accompanied by precipitation of new mineral assemblages from the incompatible-element-enriched fluid (Chakhmouradian and Zaitsev 2002). Titanite is estimated to have crystallized at temperatures near 200 °C, with weakly acidic pH, and activity of dissolved silica $\geq 10^{-4}$ (Chakhmouradian and Zaitsev 2002). These estimates agree well with the occurrence of titanite, clinochlore, and hibschite in the same paragenesis. Subsequent to the crystallization of the deuteric silicates, the silica activity and probably also pH dropped whereas $P(CO_2)$ increased, as signified by the ubiquitous precipitation of ancylite-group minerals and other late-stage carbonates (Chakhmouradian and Zaitsev 2002; Zaitsev and Chakhmouradian 2002). The stability of titanite in carbonatitic fluids is constrained by the activity of dissolved silica, pH, and $P(CO_2)$, which can be schematically expressed by the following reactions:

$$CaTiSiO_5 + 2H_2O = CaTiO_3 + H_4SiO_4^0 \quad (1)$$
$$CaTiSiO_5 + H_2O + 2H^+ = TiO_2 + Ca^{2+} + H_4SiO_4^0 \quad (2)$$
$$CaTiSiO_5 + CO_2 + 2H_2O = CaCO_3 + TiO_2 + H_4SiO_4^0 \quad (3)$$

The location of equilibria 1–3 at T = 200 °C is shown in Figure 6. Equilibrium 2 has limited significance in carbonatites because above 150° C the reaction of calcite dissociation lies at higher pH, i.e., $a(H^+)$ will be buffered by the reaction between primary (liquidus) calcite and fluid. Equilibrium 3 is more important, as signified by the occurrence of late-stage calcite (or dolomite, depending on the activities of Mg^{2+} and Fe^{2+}) and TiO_2 minerals in place of titanite in many carbonatites (for review, see Chakhmouradian and Williams 2004). As noted previously, resorption of titanite is not observed and rutile is exceedingly rare at Afrikanda, indicating that the fluid evolved within the titanite stability field. In some carbonatites, the silica activity was insufficient to stabilize titanite, and the calcite + TiO_2 assemblage developed at the expense of perovskite (e.g., Mitchell and Chakhmouradian 1998).

Compositional variation

Deuteric titanite is relatively common in carbonatitic rocks elsewhere in the Kola alkaline igneous province. In common with Afrikanda, it is typically developed as thin reaction rims on, and fracture fillings in, precursor Ti minerals, especially perovskite. For comparative purposes, microcrystic titanite from three other Kola complexes was analyzed in this work: Kovdor, Seblyavr, and Turiy Mys. All four complexes occur in an intracratonic setting, have Devonian ages, and are structurally and petrologically similar. Hence, the emplacement and evolution of these intrusions are believed to have involved broadly similar petrogenetic processes. The samples examined here are carbonatitic rocks differing in modal composition, but invariably containing cumulus Nb-bearing perovskite. Titanite, developed along fractures in the perovskite, shows moderate variation in composition owing to substitutions at both Ti and Ca sites. The highest Al and Fe contents are observed in the Kovdor sample, whereas the Seblyavr sample is Al-Fe-poor, but contains elevated levels of Na and Nb; the Turiy Mys sample is compositionally intermediate (Table 3). None of the obtained compositions approach the extent of Al, Fe, Nb, or Zr enrichment documented

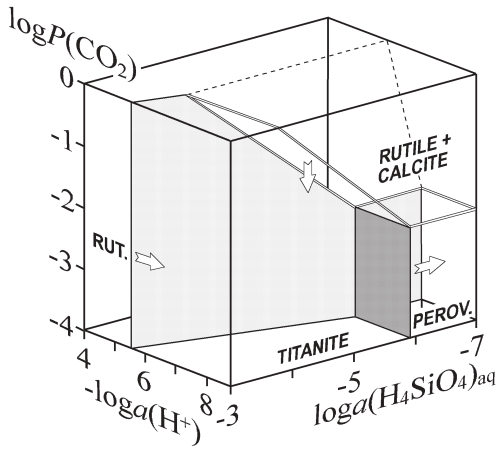

FIGURE 6. Stability fields of titanite and associated Ti minerals in carbonatitic fluids at T = 200° C and $a(Ca^{2+}) = 10^{-3}$. The titanite (perovskite) ↔ rutile equilibria are shown by the white non-transparent surfaces, titanite (perovskite) ↔ rutile + calcite equilibria by the double-contoured transparent surfaces, and perovskite ↔ titanite equilibrium by the stippled surface; the rutile + calcite field is separated from the rutile field by the calcite-out surface (dash-contoured); its continuation into the titanite stability field is omitted for clarity. Block arrows indicate where the equilibria shift with decreasing temperature. The equilibrium surfaces were located by Gibbs free-energy minimization using a self-consistent set of thermodynamic data (Bulakh et al. 1995).

TABLE 3. Representative compositions of deuteric titanite from Kola

Wt%	1	2	3	4	5	6	7
Na_2O	n.d	n.d	n.d	0.05	0.17	1.04	1.53
CaO	28.53	28.52	28.60	27.97	27.76	26.98	25.15
SrO	n.d	n.d	n.d	0.14	n.d	n.d	n.d
La_2O_3	0.06	n.d	n.d	n.d	n.d	n.d	n.d
Ce_2O_3	0.32	0.27	0.06	0.23	0.12	0.31	0.51
Nd_2O_3	0.09	0.12	n.d	0.08	n.d	n.d	n.d
TiO_2	31.50	30.52	38.08	39.04	34.42	40.05	37.52
ZrO_2	n.d	0.08	n.d	0.32	0.14	n.d	n.d
Nb_2O_5	0.50	0.64	0.10	0.62	2.12	1.27	3.73
Ta_2O_5	n.d	n.d	n.d	n.d	0.47	n.d	n.d
Fe_2O_3*	4.27	3.66	0.68	0.33	0.67	0.13	0.11
Al_2O_3	2.94	3.57	1.38	0.26	2.59	n.d	n.d
SiO_2	30.85	30.64	30.79	30.55	30.72	30.54	29.94
Total	99.06	98.02	99.69	99.59	99.18	100.32	98.49
Structural formulae calculated on the basis of 3 cations							
Na	–	–	–	0.003	0.011	0.065	0.099
Ca	0.995	1.001	0.996	0.987	0.976	0.939	0.898
Sr	–	–	–	0.003	–	–	–
La	–	–	–	–	–	–	–
Ce	0.004	0.003	0.001	0.003	0.002	0.004	0.006
Nd	0.001	0.001	-	0.001	–	–	–
Σ	1.000	1.005	0.997	0.997	0.989	1.008	1.003
Ti	0.771	0.753	0.931	0.966	0.849	0.978	0.940
Zr	–	0.001	–	0.005	0.002	–	–
Nb	0.007	0.009	0.001	0.009	0.031	0.019	0.056
Ta	–	–	–	–	0.004	–	–
Fe*	0.105	0.090	0.017	0.008	0.017	0.003	0.003
Al_{VI}	0.113	0.138	0.053	0.010	0.100	–	–
Σ	0.996	0.991	1.002	0.998	1.003	1.000	0.999
Si	1.004	1.004	1.001	1.005	1.008	0.992	0.998

Notes: Compositions: 1–2 phoscorite, Kovdor; 3–5 calcite carbonatite, Turiy Mys; 6–7 calcite carbonatite, Seblyavr.
* Total Fe expressed as Fe_2O_3; n.d = not detected.

in the Afrikanda material.

Furthermore, analysis of the literature shows that the compositional diversity of titanite from Afrikanda is unparalleled by titanite from any other locality or rock type (Fig. 5). Aluminoan titanite with up to 53 mol% $CaAlSiO_4(OH) + CaAlSiO_4F$ (14.1–14.7 wt% Al_2O_3) has been described from low- to high-grade metamorphic rocks (e.g., Franz and Spear 1985; Enami et al. 1993; Markl and Piazolo 1999). The $Al(OH)Ti_{-1}O_{-1}$ substitution is favored at low temperatures and pressures (Enami et al. 1993), which is consistent with the data presented here. Titanite with ca. 30 mol% of $CaAlSiO_4(OH)$ occurs in calc-silicate parageneses at Salton Sea, California (ibid.), and Montagne Noire, France (Gibert et al. 1990). Niobian titanite (up to 11.2 wt% Nb_2O_5) has been documented from a wide variety of rocks, including nepheline syenites, granitic pegmatites, and calc-silicate metamorphic rocks (e.g., Bernau and Franz 1987; Woolley et al. 1992; Janeczek 1996). In addition to $Ca(Al_{0.5}Nb_{0.5})SiO_5$ (up to 34 mol% at Umm Shagir, Egypt; Bernau and Franz 1987), this titanite may contain a significant proportion of $NaNbSiO_5$ (≤10 mol% in samples from Montana; Chakhmouradian and Mitchell 1999), and of Ta components, principally $Ca(Al_{0.5}Ta_{0.5})SiO_5$ (≤22 mol% at Maršikov, Czech Republic; Černý et al. 1995). Beyond Afrikanda (Chakhmouradian and Zaitsev 2002; this work), high Fe and Zr contents have been reported for titanite from minette at Bärenstein, Germany (4.3 and 6.3 wt% respective oxides: Seifert and Kramer 2003), trachytic tuff at Roccamonfina, Italy (3.5 and 2.4 wt% respective oxides; Giannetti and Luhr 1983), and nepheline syenite at Oldoinyo Lengai, Tanzania (up to 4.2 wt% ZrO_2; Dawson et al. 1995). Titanite with 3.0–3.2 wt% Fe_2O_3 is not uncommon in granitic pegmatites, nepheline syenites, and diverse metamorphic parageneses (Woolley et al. 1992; Russell et al. 1994; Uher et al. 1998; Brugger and Gieré 1999).

In addition to showing an extensive range of compositions (Figs. 4–5), the microcrystic titanite from Afrikanda is unusual in that (1) its compositional diversity is expressed on both macro- and microscale (i.e., not only among the different varieties, but also between discrete zones in the same crystal); (2) it exhibits complex zoning patterns that cannot be correlated between the different varieties; and (3) it is characteristically poor in Na, REE, and Sr, even though these elements were enriched in the parental deuteric fluid (Chakhmouradian and Zaitsev 2002, 2004). Features (1) and (2), as well as the occurrence mode of microcrystic titanite, suggest that its crystallization was restricted to small volumes of the rock affected by hydraulic fracturing and fluid-induced metasomatism, and controlled by the local major- and trace-element budget. That the titanite enriched in Nb, Zr, and Hf occurs in spatial proximity to the primary carriers of high-field-strength elements (HFSE) indicates that these elements did not form stable species in the carbonatitic fluid, and were involved primarily in mineral-forming processes next to their source.

The low levels of Na in the Afrikanda titanite are owing to the crystallization of significant quantities of Na-bearing minerals (ceroan perovskite, loparite, and sodic-calcic amphiboles) prior to the formation of titanite (Chakhmouradian and Zaitsev 2002). On the contrary, Sr remained in the fluid during the titanite precipitation, and was subsequently sequestered in carbonates, i.e., late-stage calcite, ancylite-group minerals, and strontianite. REE

was continuously extracted from the fluid prior to (perovskite, loparite, and other oxides), nearly simultaneously with (cerite), and following the crystallization of titanite (ancylite-group minerals). This differing behavior of Na^+, Sr^{2+}, and REE^{3+} cannot be explained by changes in pH and/or temperature alone, and must reflect differences in aqueous speciation of these cations.

The reasons why the Afrikanda titanite is compositionally unique and distinct from its counterparts in other carbonatites can only be speculated upon. The four different carbonatitic rocks compared in this study are petrologically similar in that they all contain primary mafic silicates and perovskite, and all underwent late-stage re-equilibration which produced deuteric titanite. The observed difference in HFSE contents between the Afrikanda material and that from Kovdor, Seblyavr, and Turiy Mys may reflect higher mobility of HFSE in the latter three cases. Carbonate or hydroxycarbonate complexes are believed to be the primary vehicle of HFSE transport in carbonatitic fluids (for a review, see Chakhmouradian and Williams 2004). In the absence of other complexing ligands (such as F^-), the solubility of HFSE will drop with decreasing pH (e.g., Aleksandrov et al. 1969; Nabivanets and Omel'chenko 1986), triggering the precipitation of deuteric Ti, Nb, and Zr minerals.

Implications for nuclear-waste disposal

Zirconium is one of the major fission and activation products in spent nuclear fuel and high-level fuel-processing waste, with ca. 20 wt% of Zr_Σ represented by the ^{93}Zr isotope with a half-life of 1.5 million years (e.g., Baetsle et al. 1999). Several crystalline hosts have been proposed for Zr immobilization in various nuclear-waste forms, including zirconolite (ideally $CaZrTi_2O_7$) in SYNROC (e.g., Ringwood et al. 1979), and titanite in tailored and glass ceramics (Hayward et al. 1986; Harker and Flintoff 1990). These two phases have comparable critical amorphization doses (ca. 10^{19} α-decay events per gram; Ewing et al. 1995; Lumpkin 2001). The recently published mineralogical studies of zirconolite from carbonatitic rocks (including Afrikanda) demonstrate that it is susceptible to late-stage hydrothermal alteration involving hydration, introduction of Si, and loss of Ca, Ti, and Zr (for an overview of this work, see Lumpkin 2001; Chakhmouradian and Williams 2004). The fluid chemistry and conditions at which this alteration occurred were probably very similar to those described above for the case of perovskite replacement by titanite at Afrikanda, where zirconolite occurs in the same paragenesis as perovskite. Hence, zirconian titanite (with at least 15 wt% ZrO_2) appears to be significantly more resistant to weakly acidic fluids with $a(H_4SiO_4^0) > 10^{-4}$ in comparison with zirconolite. It is also noteworthy here that, under the conditions of titanite crystallization in the Afrikanda silicocarbonatite, Th-rich zircon (a proposed crystalline host for Pu; Ewing 1999) was unstable and underwent extensive re-equilibration with the fluid, which involved leaching of Th and Zr, and subsequent re-deposition of the leached elements as thorite, zirconian titanite, and Ca-Na zirconosilicates (Chakhmouradian and Zaitsev 2002).

Acknowledgments

This work was supported by the Natural Sciences and Engineering Research Council of Canada, and the University of Manitoba. I am most grateful to K. Akers and R. Bormett for their help with the acquisition of Raman spectra. A. Hammond, R. Chapman, and K. Pringnitz are thanked for their assistance with sample preparation, electron-microprobe analysis, and X-ray diffraction, respectively. The manuscript benefited from constructive comments by S. Klemme and L. Groat.

References cited

Aleksandrov, I.V., Trusikova, T.A., and Tupitsyn, B.P. (1969) Niobium and tantalum in carbon dioxide solutions. Geochemistry International, 6, 558–566.

Baetsle, L.H. et al. (1999) Actinide and fission product partitioning and transmutation. Status and Assessment Report of the Nuclear Energy Agency. Available on-line at http://www.nea.fr/html/trw/docs/neastatus99/completedoc.pdf.

Bernau, R. and Franz, G. (1987) Crystal chemistry and genesis of Nb-, V-, and Al-rich metamorphic titanite from Egypt and Greece. Canadian Mineralogist, 25, 695–705.

Brugger, J. and Gieré, R. (1999) As, Sb Be and Ce enrichment in minerals from a metamorphosed Fe-Mn deposit, Val Ferrera, eastern Swiss Alps. Canadian Mineralogist, 37, 37–52.

Bulakh, A.G., Krivovichev, V.G., and Zolotarev, A.G. (1995) Mineral formulae. Thermodynamic analysis in mineralogy and geochemistry, 260 p. St. Petersburg University Press, Russia.

Černý, P., Novák, M., and Chapman, R. (1995) The $Al(Nb,Ta)Ti_{-2}$ substitution in titanite: the emergence of a new species? Mineralogy and Petrology, 52, 61–73.

Chakhmouradian, A.R. and Mitchell, R.H. (1999) Primary, agpaitic and deuteric stages in the evolution of accessory Sr, REE, Ba and Nb-mineralization in nepheline-syenite pegmatites at Pegmatite Peak, Bearpaw Mts., Montana. Mineralogy and Petrology, 67, 85–110.

Chakhmouradian, A.R. and Williams, C.T. (2004) Mineralogy of high-field-strength elements in carbonatitic rocks of the Kola Peninsula, Russia. In F. Wall and A.N. Zaitsev, Eds., Phoscorites and carbonatites from mantle to mine: The key example of the Kola Peninsula. Mineralogical Society (UK) Series, in press.

Chakhmouradian, A.R. and Zaitsev, A.N. (2002) Calcite-amphibole-clinopyroxene rock from the Afrikanda complex, Kola Peninsula, Russia: mineralogy and a possible link to carbonatites. III. Silicate minerals. Canadian Mineralogist, 40, 1347–1374.

——— (2004) Afrikanda: An association of ultramafic, alkaline and alkali-silica-rich carbonatitic rocks from mantle-derived melts. In F. Wall and A.N. Zaitsev, Eds., Phoscorites and carbonatites from mantle to mine: The key example of the Kola Peninsula. Mineralogical Society (UK) Series, in press.

Dawson, J.B., Smith, J.V., and Steele, I.M. (1995) Petrology and mineral chemistry of plutonic igneous xenoliths from the carbonatite volcano, Oldoinyo Lengai, Tanzania. Journal of Petrology, 36, 797–826.

Della Ventura, G., Bellatreccia, F., and Williams, C.T. (1999) Zr- and LREE-rich titanite from Tre Croci, Vico Volcanic complex (Latium, Italy). Mineralogical Magazine, 63, 123–130.

Enami, M., Suzuki, K., Liou, J.G., and Bird, D.K. (1993) Al-Fe^{3+} and F-OH substitutions in titanite and constraints on the P-T dependence. European Journal of Mineralogy, 5, 219–231.

Ewing, R.C. (1999) Nuclear waste forms for actinides. Proceedings of the National Academy of Sciences of the U.S.A., 96, 3432–3439.

Ewing, R.C., Weber, W.J., and Clinard, F.W. (1995) Radiation effects in nuclear waste forms for high-level radioactive waste. Progress in Nuclear Energy, 29, 63–127.

Franz, G. and Spear, F.S. (1985) Aluminous titanite (sphene) from the eclogite zone, south-central Tauern Window, Austria. Chemical Geology, 50, 33–46.

Ghose, S., Ito, Y., and Hatch, D.M. (1991) Paraelectric-antiferroelectric phase transitions in titanite, $CaTiSiO_5$: I. A high temperature X-ray diffraction study of the order parameter and transition mechanism. Physics and Chemistry of Minerals, 17, 604–610.

Giannetti, B. and Luhr, F. (1983) The white trachytic tuff of Roccamonfina Volcano (Rome Region, Italy). Contributions to Mineralogy and Petrology, 84, 235–252.

Gibert, F., Moine, B., and Gibert, P. (1990) Titanites (sphènes) alumineuses formées à basse/moyenne pression dans les gneiss à silicates calciques de la Montagne Noire. Comptes Rendus de l'Académie des Sciences, Série II, 311, 657–663.

Groat, L.A., Kek, S., Bismayer, U., Schmidt, C., Krane, H.G., Meyer, H., Nistor, L., and Van Tendeloo, G. (1996) A synchrotron radiation, HRTEM, X-ray powder diffraction, and Raman spectroscopic study of malayaite, $CaSnSiO_5$. American Mineralogist, 81, 595–602.

Harker, A.B. and Flintoff, J.F. (1990) Polyphase ceramic for consolidating nuclear waste compositions with high zirconium-cadmium-sodium content. Journal of the American Ceramic Society, 73, 1901–1906.

Hawthorne, F.C. et al. (1991) Alpha-decay damage in titanite. American Mineralogist, 76, 370–396.

Hayward, P.J., Watson, D.G., McIlwain, A.K., George, I.M., and Mitchell, S.L. (1986) Leaching studies of sphene ceramics containing substituted radionuclides. Nuclear and Chemical Waste Management, 6, 71–80.

Heyns, A.M., Harden, P.M., and Prinsloo, L.C. (2000) Resonance Raman study of the high-pressure phase transition in chromium-doped titanite, $CaTiOSiO_4$. Journal of Raman Spectroscopy, 31, 837–841.

Hole, M.J., Trewin, N.H., and Still, J. (1992) Mobility of the high field strength, rare earth elements and yttrium during late diagenesis. Journal of the Geological Society (London), 149, 689–692.

Hollabaugh, C.L. and Foit, F.F. (1984) The crystal structure of an Al-rich titanite from Grisons, Switzerland. American Mineralogist, 69, 725–732.

Janeczek, J. (1996) Nb-, Ta- and Sn-rich titanite and its alteration in pegmatites from Żólkiewka, Poland. Neues Jahrbuch für Mineralogie Monatshefte, 10, 459–469.

Kunz, M., Arlt, T., and Stolz, J. (2000) In situ diffraction study of titanite (CaTiOSiO$_4$) at high pressure and high temperature. American Mineralogist, 85, 1465–1473.

Lumpkin, G.R. (2001) Alpha-decay damage and aqueous durability of actinide host phases in natural systems. Journal of Nuclear Materials, 289, 136–166.

Markl, G. and Piazolo, S. (1999) Stability of high-Al titanite from low-pressure calcsilicates in light of fluid and host-rock composition. American Mineralogist, 84, 37–47.

Mitchell, R.H. and Chakhmouradian, A.R. (1998) Instability of perovskite in a CO_2-rich environment: examples from carbonatite and kimberlite. Canadian Mineralogist, 36, 939–952.

Muir, I.J., Metson, J.B., and Bancroft G.M. (1984) ^{57}Mössbauer spectra of perovskite and titanite. Canadian Mineralogist, 22, 689–694.

Nabivanets, B.I. and Omel'chenko, Yu.A. (1986) Carbonato-complexes of titanium(IV) in solution. Russian Journal of Inorganic Chemistry, 31, 201–203.

Peterson, T.D. (1989) Peralkaline nephelinites. I. Comparative petrology of Shombole and Oldoinyo L'engai, East Africa. Contributions to Mineralogy and Petrology, 101, 458–478.

Ringwood, A.E., Kesson, S.E., Ware, N.G., Hibberson, W., and Major, A. (1979) Immobilisation of high level nuclear reactor wastes in SYNROC. Nature, 278, 219–223.

Rodriguez-Carvajal, J. (1990) "FULLPROF" Program: Rietveld Pattern Matching Analysis of Powder Patterns. Grenoble, France.

Russell, J.K., Groat, L.A., and Halleran, A.A.D. (1994) LREE-rich niobian titanite from Mount Bisson, British Columbia: Chemistry and exchange mechanisms. Canadian Mineralogist, 32, 575–587.

Schulze, D.J. (1990) Silicate-bearing rutile-dominated nodules from South African kimberlites: Metasomatized cumulates. American Mineralogist, 75, 97–104.

Seifert, W. and Kramer, W. (2003) Accessory titanite: an important carrier of zirconium in lamprophyres. Lithos, 71, 81–98.

Shannon, R.D. (1976) Revised effective ionic radii and systematic studies of interatomic distances in halides and chalcogenides. Acta Crystallographica, A32, 751–767.

Stäuble, J. and Bayer, G. (1981a) Eignet sich Titanit zur Fixierung radioaktiver Abfälle? Schweizerische Mineralogische und Petrographische Mitteilungen, 61, 361–365.

——— (1981b) Titanit als mögliche Wirtstruktur zur Fixierung von Elementen aud radioaktiven Abfällen. Naturwissenschaften, 68, 141.

Stefanovsky, S.V., Yudintsev, S.V., Nikonov, B.S., Omelianenko, B.I., and Lapina, M.I. (2000) Isomorphic capacity of synthetic sphene with respect to Gd and U. Materials Research Society Symposium Proceedings, 608, 455–460.

Troitzsch, U., Ellis, D.J., Thompson, J., and Fitz-Gerald, J. (1999) Crystal structural changes in titanite along the join TiO-AlF. European Journal of Mineralogy, 11, 955–965.

Uher, P., Černý, P., Chapman, R., Határ, J., and Miko, O. (1998) Evolution of Nb,Ta-oxide minerals in the Prašivá granitic pegmatites, Slovakia. II. External hydrothermal Pb,Sb overprint. Canadian Mineralogist, 36, 535–545.

Villeneuve, M.E. and Relf, C. (1998) Tectonic setting of 2.6 Ga carbonatites in the Slave Province, NW Canada. Journal of Petrology, 39, 1975–1986.

Woolley, A.R., Platt, R.G., and Eby, N. (1992) Niobian titanite and eudialyte from the Ilomba nepheline syenite complex, north Malawi. Mineralogical Magazine, 56, 428–430.

Zaitsev, A.N. and Chakhmouradian, A.R. (2002) Calcite-amphibole-clinopyroxene rock from the Afrikanda complex, Kola Peninsula, Russia: mineralogy and a possible link to carbonatites. II. Oxysalt minerals. Canadian Mineralogist, 40, 103–120.

MANUSCRIPT RECEIVED DECEMBER 15, 2003
MANUSCRIPT ACCEPTED MAY 11, 2004
MANUSCRIPT HANDLED BY LEE GROAT

APPENDIX 1

Names and empirical formulae of some less-common minerals cited in the text: ancylite-(Ce) $(Sr,Ca)_{4-x}LREE_x(CO_3)_4(OH)_x\cdot(4-x)H_2O$; baddeleyite ZrO_2; cerite-(Ce) $(LREE,Ca)_9(Fe,Al)(SiO_4)_6(SiO_3OH)(OH)_3$; gittinsite $CaZrSi_2O_7$; hibschite $Ca_3(Al,Fe)_2(SiO_4)_{3-x}(OH)_{4x}$; loparite-(Ce) $(Na,LREE,Ca,Th)(Ti,Nb)O_3$; shorlomite $Ca_3(Ti,Fe,Mg)_2(Si,Fe,Al)_3O_{12}$; zirconolite $(Ca,LREE)Zr(Ti,Nb,Fe)_2O_7$.